

Elliptic Flow from Minijet Production in Heavy Ion Collisions

Yuri V. Kovchegov*^a and Kirill L. Tuchin^{† b}

^a*Department of Physics, University of Washington, Box 351560
Seattle, WA 98195*

^b*Institute for Nuclear Theory, University of Washington, Box 351550
Seattle, WA 98195*

March, 2002

Abstract

We calculate the contribution to the elliptic flow observable v_2 from two-particle correlations in minijet production in ultrarelativistic heavy ion collisions. We use a minijet production cross section derived in a model inspired by saturation approach to high energy scattering. Resulting differential elliptic flow $v_2(p_T)$ is an increasing function of p_T for transverse momenta below the saturation scale Q_s . At higher transverse momenta ($p_T > Q_s$) differential flow stops growing and becomes approximately constant, reproducing the elliptic flow saturation data reported by STAR. The centrality dependence of the minijet contribution to v_2 is also in good agreement with the data.

*e-mail: yuri@phys.washington.edu

†e-mail: tuchin@phys.washington.edu

1 Introduction

Ultrarelativistic heavy ion collisions provide us interesting new information on QCD under extreme conditions. Different stages of the collisions probe QCD in different regimes: early times are likely to be characterized by strong saturated gluonic fields [1, 2] while creation of quark-gluon plasma (QGP) is an attractive possibility in the later stages of the collisions [3]. To be able to understand the experimental data generated in the collisions one has to learn to disentangle between the contributions of these two (in principle) different physical processes to heavy ion observables.

The strong quasi-classical gluon fields are produced in the early stages of the collisions due to high transverse densities of color charges in the wave functions of the Lorentz-contracted nuclei [2, 4, 5, 6, 7, 8]. The typical color charge density is characterized by the *saturation* scale Q_s^2 , which grows with nuclear atomic number and with energy of the collision [1, 2, 9, 10, 11]. While being coherent over large longitudinal distances these quasi-classical fields have a rather short coherence length in the transverse direction, of the order of the inverse saturation scale $1/Q_s$. Saturation-inspired models have been quite successful in describing the emerging RHIC data on rapidity and centrality dependence of the total charged multiplicity of the produced particles [12, 13].

In the later stages of the collisions gluons and quarks generated by the quasi-classical fields are likely to reach kinetic, and, possibly, chemical thermal equilibrium, producing the quark-gluon plasma (QGP) [3, 14, 15, 16]. To be able to study this new state of matter one should be able to distinguish the contributions to physical observables of the collective phenomena due to QGP from the effects of strong gluonic fields of the early stages. Ideally one should try to construct observables which would be sensitive only to one type of physics while being independent of the other. An example of such observables are the long range rapidity correlations predicted in [17], which are almost entirely due to the dynamics of initial conditions.

In this paper we would like to study the contribution of the quasi-classical gluonic fields to the elliptic flow observable v_2 , defined as the second Fourier moment of the azimuthal momentum distribution of the produced particles [18]. Elliptic flow reflects anisotropy of the transverse momentum distribution of the produced particles with respect to reaction plane. There has been a large amount of elliptic flow data produced in the heavy ion collisions at SPS [19, 20] and RHIC [21, 22, 23]. While the majority of these data are in good agreement with hydrodynamic simulations [24, 25], the emerging new STAR data on differential elliptic flow $v_2(p_T)$ at high p_T seems to deviate from hydrodynamic predictions [26]. Instead of continuing to increase with p_T the flow variable $v_2(p_T)$ saturates to approximately a constant above $p_T = 1.5$ GeV [26]. The data goes up to $p_T \approx 4.5$ GeV [26]. It is natural to expect that at such high momenta the hard (perturbative) physics should be responsible for the underlying strong interactions dynamics*. This led the authors of [27] to propose a model of interplay of soft and hard interactions in v_2 : while the low momentum part of v_2 was still described by hydrodynamic calculations the high p_T part was described by medium-induced radiative energy loss of partons [28] which would generate azimuthal anisotropy in momentum space due to coordinate space anisotropy of the overlap region. The resulting flow observable would saturate at some relatively large p_T and then would decrease with increasing p_T .

*Very recently an attempt was made in [29] to explain the high- p_T elliptic flow using pure classical gluon fields of the nuclei [6] yielding the elliptic flow which is too small to explain the data.

Here we are going to propose a model of a non-flow particle production mechanism generating an elliptic flow observable v_2 which would go to a constant at large p_T and would stay approximately constant as p_T increases. Let us picture particle production at the early stages of a nuclear collision at high energy. In the first approximation high- p_T particles are produced independent of each other. We can illustrate this in the framework of the saturation approach to nuclear collisions: there the gluon fields are coherent over very short transverse distances of the order of $1/Q_s$, with $Q_s \gg \Lambda_{QCD}$. The high energy wave function of a large nucleus can be viewed in the transverse plane as consisting of many independent gluon fields each of them occupying a transverse area $1/Q_s^2$. (In the longitudinal direction each classical field is of course coherent over the whole nucleus [2] and this way the nucleus can be considered as “sliced” into narrow pipes with diameter $1/Q_s$.) Therefore a collision with the overlap transverse area of the two nuclei S_\perp could be pictured as at least $S_\perp Q_s^2$ independent (sub)collisions. For sufficiently central heavy ion collisions $S_\perp Q_s^2 \sim N_{part} \gg 1$, where N_{part} is the number of nucleons participating in the collision. At the leading order in this large parameter $S_\perp Q_s^2$ the two-particle multiplicity distribution factorizes into a product of two single-particle multiplicity distributions. Correlation between a pair of particles in the perturbative production mechanism happens when both particles are produced in the same subcollision, i.e., at the same impact parameter. Therefore these correlations appear at the subleading in $S_\perp Q_s^2$ order and are suppressed by a power of $S_\perp Q_s^2$. We are going to argue below that this does not prevent them from significantly contributing to elliptic flow observable.

The standard definition of differential elliptic flow is [30, 31, 32, 33, 35]

$$v_2(p_T) = \left\langle e^{2i(\phi_{p_T} - \Phi_R)} \right\rangle = \left\langle \cos 2(\phi_{p_T} - \Phi_R) \right\rangle \quad (1)$$

where ϕ_{p_T} is the azimuthal angle of the produced particle with the value of transverse momentum p_T , Φ_R is the azimuthal angle of the reaction plane and the brackets denote statistical averaging over different events which leaves non-zero only the contribution of the cosine in Eq. (1). The reaction plane is determined by averaging over particles produced in a heavy ion collision with certain weights designed to optimize the reaction plane resolution [31]. Let us imagine that the particle with momentum p_T in Eq. (1) was produced in the same subcollision with some other particle, which contributed to determination of the reaction plane angle Φ_R . Then the particle p_T would be correlated with the reaction plane by these non-flow azimuthal correlations. The averaged over events correlations do not disappear at high p_T , as will be shown below. Therefore the elliptic flow observable v_2 may be potentially sensitive to the non-flow correlations originating from minijet production in the initial conditions. To avoid this problem the authors of [32] (see also [34]) introduced a cumulant approach to flow analysis. In terms of the saturation model contribution of minijets to higher order cumulants defined in [32, 34] is suppressed by powers of $S_\perp Q_s^2 \sim N_{part}$. This led the authors of [32, 34] to suggest that the high-cumulant flow analysis would be relatively free of minijet effects compared to standard flow analysis.

There are certain potential dangers in this conclusion which have to be addressed in an explicit calculation. One is that for peripheral collisions $S_\perp Q_s^2 \sim N_{part}$ is not such a large number and therefore minijet effects should not be suppressed anymore. From the experimental data [21, 22, 23] we know that elliptic flow is strongest in peripheral collisions making the minijet contribution also large. Another potentially dangerous question is whether the parameter $S_\perp Q_s^2$ appears in actual calculations with some numerically small prefactor making inverse powers of

$S_{\perp}Q_s^2$ not too small. After all the observed differential v_2 is also not a very large quantity being of the order of 10 – 15% at RHIC and may be very sensitive to such corrections.

To clarify the questions mentioned above we are going to perform an explicit calculation of the minijet contribution to the elliptic flow observable. The paper is structured as follows. In Sect. 2 we show that the standard determination of flow employing Eq. (10) and the flow extracted from the 2nd cumulant proposed in [32, 33, 34] should yield the same result for v_2 for a trivial choice of weights. This result was confirmed by an explicit flow analysis using two different methods at STAR giving almost the same result for v_2 [36].

The second order cumulant from [32, 34] is nothing but a two-particle correlation function, a contribution to which from the minijet production is calculated in Sect. 3. To construct a model of minijet production which incorporates both hard and soft physics we have used k_T factorized expression for two-jet production with the unintegrated gluon distributions given by the quasi-classical Glauber-Mueller expression [37, 38, 39, 40, 41, 5]. These gluon distributions are characterized by the saturation scale $Q_s \gg \Lambda_{QCD}$ which insures applicability of small coupling approaches down to rather small transverse momenta of the produced particles. Our model of course does not yield us the exact two-particle production cross section, but gives a realistic approximation similar to the one used in [12, 13] to describe the multiplicity distributions at RHIC. An exact calculation of double inclusive minijet production in the quasi-classical framework appears to be rather complicated and is left for further research: even the single inclusive cross section has not been yet unambiguously theoretically determined, despite the extensive efforts [7, 8].

In Sect. 3 we calculate the differential flow observable resulting from these two-particle correlations. Our final result is given in Eq. (40). The obtained differential elliptic flow $v_2(p_T)$ starts increasing as a power of p_T for small $p_T \ll Q_s$ (see Eq. (41)) and then saturates to a slow logarithmic growth for $p_T \gg Q_s$ (see Eq. (42)). We also derive the centrality dependence of the minijet flow contribution (see Eq. (45)).

In Sect. 4 after making some simple assumptions about the gluon distributions employed in the minijet production cross section we fit the differential elliptic flow STAR data [26] using the flow from Eq. (40) with $\alpha_s = 0.3$, $Q_s = 1 \text{ GeV}^2$. These values are in agreement with the ones used in the saturation-inspired analysis of the multiplicity data in [12, 13]. The fit is shown in Fig. 3. We can also fit the centrality dependence of v_2 with our minijet model by noting that the integrated flow should scale as $v_2(B) \sim 1/\sqrt{S_{\perp}Q_s^2} \sim 1/\sqrt{N_{part}}$ (see Fig. 4).

We discuss the results in Sect. 5 by stating that while a more involved numerical analysis is still needed to analyze the emerging RHIC data on elliptic flow we have demonstrated that the contribution of minijets to the standard flow analysis is very large, possibly accounting for most of high- p_T data. Thus it appears that the standard flow analysis is heavily “contaminated” by minijets which prevent direct measurements of the contribution of collective QGP effects to elliptic flow. At the same time flow analysis seems to be rather sensitive to details of saturation physics and could be used for determination of nuclear saturation scales.

2 Different Methods of Flow Analysis

In [32] Borghini et al proposed a new and interesting approach to flow analysis employing higher order cumulants. Let us outline some important features of the approach presented in

[32] for the lowest order cumulant. The second order cumulant is defined for two particles with azimuthal angles ϕ_1 and ϕ_2 as [32, 33, 34]

$$\langle\langle e^{2i(\phi_1-\phi_2)} \rangle\rangle = \langle e^{2i(\phi_1-\phi_2)} \rangle - \langle e^{2i\phi_1} \rangle \langle e^{-2i\phi_2} \rangle. \quad (2)$$

The average $\langle e^{2i\phi_1} \rangle$ vanishes since the angle here is measured in the laboratory and heavy ion collisions are azimuthally symmetric after averaging over many events. For flow correlations this means that the angle in $\langle e^{2i\phi_1} \rangle$ is not measured with respect to reaction plane, but with respect to some fixed direction in the detector. Assuming that the particles 1 and 2 are correlated with each other only through the flow correlations with the reaction plane the authors of [33] wrote

$$\langle\langle e^{2i(\phi_1-\phi_2)} \rangle\rangle = \langle e^{2i(\phi_1-\phi_2)} \rangle = \langle e^{2i(\phi_1-\Phi_R)} e^{2i(\Phi_R-\phi_2)} \rangle = \langle v_2 \rangle^2, \quad (3)$$

where the definition of elliptic flow from Eq. (1) was employed. A new method for measuring elliptic flow was proposed in [32] using the two particle (and higher order) cumulants of Eq. (3). If we fix the transverse momentum of particle 1 to be p_T and average over all momenta of the particle 2 over many events then as one can see from Eq. (3)

$$\langle e^{2i(\phi_1(p_T)-\phi_2)} \rangle = v_2(p_T) \langle v_2 \rangle \quad (4)$$

with $\langle v_2 \rangle$ the elliptic flow variable averaged over all p_T . At the same time if we do not impose any restrictions on the transverse momenta of both particles we get [33]

$$\langle e^{2i(\phi_1-\phi_2)} \rangle = \langle v_2 \rangle^2. \quad (5)$$

From Eqs. (4) and (5) noting that only cosine components of the exponents survive the averaging we obtain the following expression for differential elliptic flow [33]

$$v_2(p_T) = \frac{\langle \cos(2(\phi_1(p_T) - \phi_2)) \rangle}{\sqrt{\langle \cos(2(\phi_1 - \phi_2)) \rangle}}. \quad (6)$$

Let us define the event-averaged two-particle multiplicity distribution function

$$P(k_1, k_2, \underline{B}) = \frac{dN}{d^2k_1 dy_1 d^2k_2 dy_2}(\underline{B}), \quad (7)$$

where the transverse momenta of the particles are \underline{k}_1 and \underline{k}_2 , while y_1 and y_2 are their rapidities and we average over all events with the impact parameter \underline{B} between the two nuclei. This distribution can be written as a sum of uncorrelated and correlated terms

$$P(k_1, k_2, \underline{B}) = \frac{dN}{d^2k_1 dy_1} \frac{dN}{d^2k_2 dy_2} + \frac{dN_{corr}}{d^2k_1 dy_1 d^2k_2 dy_2}, \quad (8)$$

where we suppressed the impact parameter dependence. The correlated term in Eq. (8) is usually much smaller than the uncorrelated one as it is suppressed by a power of $Q_s^2 S_\perp \sim N_{part}$. Using Eq. (7) we rewrite Eq. (6) as

$$v_2(k_1, \underline{B}) = \frac{\int d^2k_2 dy_2 d\phi_1 dy_1 P(k_1, k_2, \underline{B}) \cos(2(\phi_1 - \phi_2))}{\int d^2k_2 dy_2 d\phi_1 dy_1 P(k_1, k_2, \underline{B})}$$

$$\times \left(\frac{\int d^2k_1 dy_1 d^2k_2 dy_2 P(k_1, k_2, \underline{B})}{\int d^2k_1 dy_1 d^2k_2 dy_2 P(k_1, k_2, \underline{B}) \cos(2(\phi_1 - \phi_2))} \right)^{1/2}, \quad (9)$$

where we have relabeled the transverse momenta of the particles to be \underline{k}_1 and \underline{k}_2 . Eq. (9) gives us a way of calculating elliptic flow from two-particle correlation functions. Higher order cumulants would yield us ways of calculating flow from higher order particle correlations [32], though one can not go to arbitrary high order cumulants due to lack of statistics there. An analysis of RHIC data has been performed at STAR [36] using both conventional and cumulant approaches explicitly demonstrating that the flow obtained by the second cumulant technique of Eq. (9) is consistent with the flow extracted using conventional techniques. That is the approach of Eq. (9) is equivalent to the conventional flow analysis. To see this let us first note that in the actual standard flow analysis one has to take into account the resolution in the event plane determination [31]. This would modify Eq. (1) giving [31, 21]

$$v_2(p_T) = \frac{\langle \cos(2(\phi_{p_T} - \Psi_R)) \rangle}{\sqrt{2 \langle \cos(2(\Psi_R^a - \Psi_R^b)) \rangle}} \quad (10)$$

where Ψ_R^a and Ψ_R^b are the event plane angles determined in two different sub-events labeled a and b with the particle multiplicity $N/2$ in each of them while Ψ_R is the event plane angle determined in the full event with multiplicity N [31]. Eq. (10) is quite similar to Eq. (6). To show that the two equations are almost equivalent let us go back to exponential notation and rewrite the numerator of Eq. (6) as

$$\langle \cos(2(\phi_1(p_T) - \phi_2)) \rangle = \left\langle \left\langle e^{2i(\phi_1(p_T) - \phi_2(k_T))} \right\rangle_{\text{all } k_T \neq p_T} \right\rangle_{\text{events}} \quad (11)$$

where we first average over all particles (with various k_T) in a given event other than the chosen particle with momentum p_T , just like in the standard flow analysis [22], and then average over all events. On the other hand, the azimuthal angle of the reaction plane Ψ_R in Eq. (10) can be defined by

$$Q_N e^{-2i\Psi_R} = \left\langle e^{-2i\phi_{k_T}} \right\rangle_{\text{all } k_T \neq p_T}, \quad (12)$$

where Q_N is a real number. If one neglects correlations between the particles and multiplies Eq. (12) by its complex conjugate avergaing over events with the same total multiplicity N one easily gets $\langle Q_N^2 \rangle = 1/N$ [32]. Therefore at the leading order in N we have (for large N) $Q_N \sim 1/\sqrt{N}$. In Eq. (12) we for the moment forget about the transverse momentum cutoffs imposed in event plane determination and subtleties related to different choices of weights and detector imperfections. Substituting Eq. (12) into the numerator of Eq. (10) we obtain

$$\begin{aligned} \langle \cos(2(\phi_{p_T} - \Psi_R)) \rangle_{\text{events}} &= \left\langle e^{2i(\phi_{p_T} - \Psi_R)} \right\rangle_{\text{events}} = \left\langle \frac{1}{Q_N} \left\langle e^{2i(\phi_{p_T} - \phi_{k_T})} \right\rangle_{\text{all } k_T \neq p_T} \right\rangle_{\text{events}} \\ &\approx \frac{1}{\langle Q_N \rangle} \left\langle \left\langle e^{2i(\phi_{p_T} - \phi_{k_T})} \right\rangle_{\text{all } k_T \neq p_T} \right\rangle_{\text{events}} \end{aligned} \quad (13)$$

where we assumed that for a fixed impact parameter collisions the particle multiplicity N (and, therefore, Q_N) is independent of two-particle correlations. Eq. (13) is identical to Eq. (11) up

to a factor of $1/\langle Q_N \rangle$. Similarly one can show that the denominators in Eqs. (10) and (6) are equal to each other up to a factor of $\sqrt{2/\langle Q_{N/2}^2 \rangle}$:

$$2 \left\langle \cos(2(\Psi_R^a - \Psi_R^b)) \right\rangle_{events} = 2 \left\langle \frac{1}{Q_{N/2}^2} \left\langle e^{2i(\phi_{k_{T1}} - \phi_{k_{T2}})} \right\rangle_{all\ different\ k_{T1}, k_{T2}} \right\rangle_{events} \\ \approx \frac{2}{\langle Q_{N/2}^2 \rangle} \langle \cos(2(\phi_1 - \phi_2)) \rangle. \quad (14)$$

Recalling that for large multiplicities $\langle Q_N \rangle \sim 1/\sqrt{N}$ we see that at the leading order in N : $\sqrt{\langle Q_{N/2}^2 \rangle}/\sqrt{2} \langle Q_N \rangle \approx \langle Q_{N/2} \rangle/\sqrt{2} \langle Q_N \rangle \approx 1$. Extra factors in the numerator and denominator of Eq. (10) cancel reducing it to Eq. (6). Thus we showed that Eqs. (10) and (6) are identical in the limit of large multiplicity N . We have proven that the standard definition of flow from Eq. (10) is equivalent to the definition introduced in [32, 34] given here by Eq. (6)). Therefore in order to calculate the differential elliptic flow $v_2(p_T)$ we need only to calculate the two-particle correlation function $P(k_1, k_2, \underline{B})$ and substitute it into Eq. (9).

3 Calculation of v_2

To calculate the two-particle correlation coefficient in Eq. (8) one needs to know single and double particle multiplicity distributions. While the quasi-classical single particle production mechanisms in heavy ion collisions have been extensively studied [6, 7, 8], the double inclusive particle production has not been calculated yet. One needs to calculate production of a pair of particles with comparable transverse momenta $|\underline{k}_1| \sim |\underline{k}_2| \sim Q_s$ and rapidities $y_1 \sim y_2$ in the framework of McLerran-Venugopalan model [7], that is resumming all powers of Q_s^2/k_\perp^2 [4, 38, 8]. Unlike the single gluon production this process involves an extra gluon and can not be described by the classical field methods of [6, 7, 8]. At the lowest order in Q_s^2/k_\perp^2 the two gluon production amplitude is equivalent to the real part of NLO BFKL kernel [42, 43] and is rather sophisticated [44]. Going beyond leading order in Q_s^2/k_\perp^2 appears to be tremendously complicated and we will not address this problem here. Instead we are going to construct a model of correlated two-particle production employing quasi-classical gluon distributions from [5, 38] in the production formula inspired by collinear factorization [40, 41], similar to how it was done in [12, 13] in describing the multiplicity data at RHIC. We would also assume that in any given event either $y_1 \gg y_2$ or $y_1 \ll y_2$. Of course this assumption does not hold in actual flow analyses [22, 23, 21] and we are making it just to simplify the calculations. While, as discussed above, a more detailed calculation would still be required to obtain an exact expression for the correlation coefficient in Eq. (8), we believe that it would only introduce numerical corrections to our approach leaving qualitative results the same.

Consider inclusive production of one or two gluons in scattering of two quarks at high energy as shown in Fig. 1, where the blobs denote effective Lipatov vertices. It is convenient to use the Sudakov decomposition of gluons' four-momenta:

$$q_i = \alpha_i p_1 + \beta_i p_2 + \underline{q}_i, \quad i = 1, 2, 3. \quad (15)$$

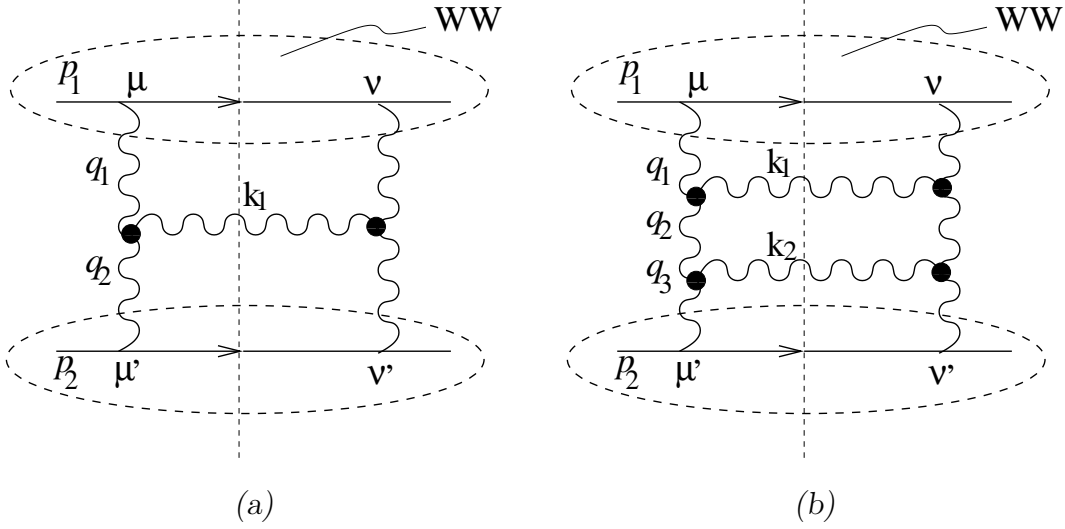


Figure 1: (a) One- and (b) two-gluon production amplitudes. Thick dots denote Lipatov vertices.

In Fig. 1(a) the dominant contribution stems from the multi-regge kinematical region where $\alpha_1 \gg \alpha_2$ and $\beta_2 \gg \beta_1$. Using Ward identities the t -channel gluon propagators can be written as

$$D^{\mu\nu}(q_i) = \frac{2 \underline{q}_i^\mu \underline{q}_i^\nu}{s \alpha_i \beta_i}, \quad (16)$$

where $s = 2(p_1 \cdot p_2)$ is center-of-mass energy squared. With this representation of the t -channel gluon propagator effective Lipatov's vertex [42] for s -channel gluon production (black blobs in the Fig. 1) reduces to the usual three-gluon vertex $\Gamma_{\mu\nu}^\rho$ and can be easily calculated:

$$L^\rho = \underline{q}_1^\mu \underline{q}_2^\nu \Gamma_{\mu\nu}^\rho = \frac{1}{2} \alpha_1 \beta_2 s \left[\left(\alpha_1 + \frac{2q_1^2}{\beta_2 s} \right) p_1^\rho + \left(\beta_2 + \frac{2q_2^2}{\alpha_1 s} \right) p_2^\rho - (\underline{q}_1 + \underline{q}_2)^\rho \right]. \quad (17)$$

In our calculation we will need the square of Lipatov's vertex given by

$$(L^\rho)^2 = \alpha_1 \beta_2 s \underline{q}_1^2 \underline{q}_2^2. \quad (18)$$

Using Eq. (16), Eq. (17), Eq. (18) and the four-dimensional momentum element decomposition

$$d^4 q_i = \frac{s}{2} d^2 \underline{q}_i d\alpha_i d\beta_i \quad (19)$$

we evaluate the single and double distribution of the produced particles shown in Fig. 1

$$\frac{dN}{d^2 k_1 dy_1} = \frac{\alpha_s^3}{\pi^2} \frac{2 C_F A^2}{S_\perp \underline{k}_1^2} \int d^2 q_1 \frac{1}{\underline{q}_1^2 (\underline{k}_1 - \underline{q}_1)^2}, \quad (20)$$

$$\frac{dN_{corr}}{d^2 k_1 dy_1 d^2 k_2 dy_2} = \frac{\alpha_s^4}{\pi^4} \frac{N_c C_F A^2}{S_\perp \underline{k}_1^2 \underline{k}_2^2} \int d^2 q_1 \frac{1}{\underline{q}_1^2 (\underline{k}_1 + \underline{k}_2 - \underline{q}_1)^2}, \quad (21)$$

where we changed variables to $\underline{k}_1 = \underline{q}_1 - \underline{q}_2$, $\underline{k}_2 = \underline{q}_2 - \underline{q}_3$ (the momenta of produced gluons). Throughout the paper we assume for simplicity that the nucleus has a cylindrical shape with radius R and “height” $2R$ and the axis of the cylinder coincides with the collision axis. $S_\perp = S_\perp(\underline{B})$ is the nucleus overlap transverse area which depends on nuclei relative impact parameter \underline{B} . We assume that colliding nuclei are identical having atomic number A each.

In fact colliding quarks in Fig. 1 are not free but confined inside nucleons. If momenta of produced gluons are higher than all scales characterizing the nucleus (including Q_s) we can use k_t -factorization to write the distributions from Eq. (20) and Eq. (21) as convolutions of hard amplitudes with parton distributions in nuclei which are predominantly gluonic in the high energy region $s \gg t$. Employing the relation [38]

$$xG_A(x, \underline{q}^2) = A xG(x, \underline{q}^2) = A \frac{\alpha_s C_F}{\pi} \ln(\underline{q}^2/\mu^2), \quad (22)$$

with μ some non-perturbative cutoff the one and two-particle distributions can be written as [45]

$$\frac{dN}{d^2k_1 dy_1} = \frac{2\alpha_s}{C_F S_\perp} \frac{1}{\underline{k}_1^2} \int d^2q_1 \frac{dxG_A}{dq_1^2} \frac{dxG_A}{d(\underline{k}_1 - \underline{q}_1)^2} \quad (23)$$

$$\frac{dN_{corr}}{d^2k_1 dy_1 d^2k_2 dy_2} = \frac{N_c \alpha_s^2}{\pi^2 C_F S_\perp} \frac{1}{\underline{k}_1^2 \underline{k}_2^2} \int d^2q_1 \frac{dxG_A}{dq_1^2} \frac{dxG_A}{d(\underline{k}_1 + \underline{k}_2 - \underline{q}_1)^2}. \quad (24)$$

As was argued in the Introduction, if the number of partons in each nuclei is large enough then their mutual interactions must be taken into account. This may happen either due to increase of parton density in each nucleon by subsequent emission of gluons in course of quantum evolution as collision energy increases [9, 11] or due to enhancement of nucleon parton density in a large nucleus by the atomic number A [2, 37, 4]. The latter effect leads to creation of the non-Abelian Weiszäcker-Williams (WW) field $\underline{A}^{WW}(\underline{z})$ of the nucleus which is a strong classical gluon field already at moderate energies [4, 5]. The WW field gives rise to the unintegrated gluon distribution given by [5, 38]

$$\begin{aligned} \frac{dxG_A(x, \underline{q}^2)}{dq^2} &= \frac{2}{(2\pi)^2} \int d^2\underline{z} e^{-i\underline{z}\cdot\underline{q}} \int d^2\underline{b} \text{Tr} \langle \underline{A}^{WW}(\underline{0}) \underline{A}^{WW}(\underline{z}) \rangle \\ &= \frac{2}{\pi(2\pi)^2} \int d^2\underline{z} e^{-i\underline{z}\cdot\underline{q}} \frac{S_\perp C_F}{\alpha_s \underline{z}^2} \left(1 - e^{-\frac{1}{4}\underline{z}^2 Q_s^2}\right), \end{aligned} \quad (25)$$

where \underline{b} is the gluon’s impact parameter (which we can trivially integrate over in a cylindrical nucleus) and

$$Q_s^2(\underline{z}) = \frac{4\pi^2 \alpha_s N_c}{N_c^2 - 1} \rho xG(x, 1/\underline{z}^2) T(\underline{b}), \quad (26)$$

with $\rho = A/[2\pi R^3]$ the atomic number density in the cylindrical nucleus with atomic number A , and $T(\underline{b})$ the nucleus profile function equal to $2R$ for the cylindrical nucleus considered here. This provides the initial condition to the nonlinear quantum evolution of the gluon distribution with energy in the high parton density region [9]. Q_s is a scale at which nonlinear nature of the gluon field becomes evident. We suggest using the classical expression Eq. (25) as an approximation to the exact gluon field of the nucleus. This is a justified approximation as long as $\alpha_s \ln s \lesssim 1$, i.e., when corrections due to quantum evolution are small.

It is usually assumed that k_T -factorization holds in high parton density regime as well as in the linear one [39]. Phenomenological models for heavy ion collisions which employ this assumption together with nonlinear evolution for gluon distributions proved to be successful in describing experimental data at SPS and RHIC [13]. This implies that the use of k_T -factorization is a quite good approximation for the SPS and RHIC kinematical regions even for $k_T < Q_s$. Therefore substituting Eq. (25) into Eq. (23) and into Eq. (24) we obtain the following expressions for the single and double gluon distributions

$$\frac{dN}{d^2k_1 dy_1} = \frac{C_F S_\perp}{\alpha_s \underline{k}_1^2} \frac{4 K_1}{\pi^3} \int_0^\infty \frac{dz}{z^3} J_0(k_1 z) \left(1 - e^{-z^2 Q_s^2/4}\right)^2, \quad (27)$$

$$\frac{dN_{corr}}{d^2k_1 dy_1 d^2k_2 dy_2} = \frac{N_c C_F S_\perp}{\underline{k}_1^2 \underline{k}_2^2} \frac{K_2}{\pi^6} \int d^2 \underline{z} \frac{1}{\underline{z}^4} e^{-i\underline{z} \cdot (\underline{k}_1 + \underline{k}_2)} \left(1 - e^{-z^2 Q_s^2/4}\right)^2, \quad (28)$$

where the saturation scales in both nuclei are the same since the nuclei are cylindrical and identical. Generalization of Eqs. (27) and (28) to a spherical nucleus is straightforward.

We have to point out again that the single particle distribution is, in principle, known better than displayed here in Eq. (27) [8]. For instance the distribution in Eq. (27) is not infrared safe, while the correct distribution derived in [8] has no infrared divergences. However, as we need both single and double particle distributions to obtain elliptic flow using Eq. (9) we should calculate both of them in the framework of the same model. Since the exact calculation of the double gluon distribution does not seem feasible at the moment we have to calculate both distributions in the same k_T -factorization approach inserting K -factors K_1 and K_2 to correct the normalization of the approximation to include higher order corrections [13], which we have done in Eqs. (27) and (28). The value of the K -factors will be fixed later. We will determine K_1 by comparing particle multiplicity per unit rapidity (dN/dy) resulting from Eq. (27) to the total multiplicity observed at RHIC [13]. To fix K_2 we consider two-particle production cross section, which is proportional to the two-particle multiplicity distribution function $P(k_1, k_2, \underline{B})$ from Eq. (8). In the limit of large transverse momentum $k_1 \sim k_2 \sim p_T$ the second term in Eq. (8) given by Eq. (28) falls off at most as $1/p_T^6$ and has a collinear singularity $\underline{k}_1 + \underline{k}_2 = 0$. Therefore it dominates over the first term in Eq. (8) given by Eq. (27) squared, which gives a $1/p_T^8$ fall off of the cross section. For large $\underline{k}_1 = -\underline{k}_2$ Eq. (8) and, therefore, Eq. (28) should match onto the corresponding collinear factorization expression for back-to-back jets [40, 41, 45, 46, 47]. To fix the normalization we expand the term in the parentheses of Eq. (28) to the lowest order and integrate over one of the transverse momenta obtaining

$$\frac{d\sigma_{corr}}{dp_T^2 dy_1 dy_2} = K_2 \frac{9 \pi \alpha_s^2}{4 p_T^4} [xG(x, p_T^2)]^2 \quad (29)$$

in agreement with collinear factorization result at mid-rapidity [40, 41, 46, 47]. We put $N_c = 3$ explicitly in Eq. (29). Collinear factorization models [40, 41, 46, 47] are rather successful in describing the high- p_T particle spectra in hadronic and heavy ion collisions when putting $K_2 = 2$ to correct the lowest order perturbative expression for next-to-leading order effects. For our model to be in agreement with these high- p_T data we will have to also put $K_2 = 2$ when trying to describe the flow data in the next section. We have to note that since the gluon distributions in Eq. (25) do not include DGLAP [48] evolution in them and Eq. (28) does not have jet quenching effects [27, 28, 47] in it our model can not be applied to describe the high- p_T

spectra and a complete DGLAP-evolved gluon distributions along with jet quenching should be used in a more detailed numerical treatment of the problem as was done for particle spectra in [40, 41, 46, 47].

Substituting Eqs. (27) and (28) into Eq. (8) we are ready to calculate $v_2(p_T, \underline{B})$. To calculate the integral in the numerator of the first line of Eq. (9) we note that only the correlated part of $P(k_1, k_2, \underline{B})$ (the second term in Eq. (8)) contributes there. Let us denote the angle between two-vectors \underline{z} and \underline{k}_1 by θ and the angle between \underline{k}_2 and \underline{k}_1 by ϕ_2 . The third angle defining direction of \underline{k}_1 is free, so we can just integrate over it obtaining a factor of 2π . Plugging Eq. (28) into Eq. (8) and using the latter in Eq. (9) we get

$$\begin{aligned}
& \int d^2k_2 d\phi_1 P(k_1, k_2, \underline{B}) \cos(2(\phi_1 - \phi_2)) = \int d^2k_2 d\phi_1 \frac{dN_{corr}}{d^2k_1 dy_1 d^2k_2 dy_2} \cos(2(\phi_1 - \phi_2)) \\
&= \frac{N_c C_F S_\perp}{\underline{k}_1^2} \frac{K_2}{\pi^5} \int \frac{dz}{z^3} d\theta \frac{dk_2^2}{k_2^2} \left(1 - e^{-z^2 Q_s^2/4}\right)^2 \int_0^{2\pi} d\phi_2 e^{-izk_2 \cos(\phi_2 - \theta)} e^{-izk_1 \cos \theta} \cos 2\phi_2 \\
&= \frac{N_c C_F S_\perp}{\underline{k}_1^2} \frac{4 K_2}{\pi^3} \int \frac{dz}{z^3} \frac{dk_2^2}{k_2^2} \left(1 - e^{-z^2 Q_s^2/4}\right)^2 J_2(k_1 z) J_2(k_2 z) \\
&= \frac{N_c C_F S_\perp}{\underline{k}_1^2} \frac{4 K_2}{\pi^3} \int_0^\infty \frac{dz}{z^3} \left(1 - e^{-z^2 Q_s^2/4}\right)^2 J_2(k_1 z). \tag{30}
\end{aligned}$$

To calculate the integral in the denominator of the first line of Eq. (9) we first note that the final state multiplicity per unit rapidity in heavy ion collisions was calculated in [8] (see also [49]) and reads

$$\frac{dN}{dy} = c \frac{S_\perp C_F Q_s^2}{\alpha_s 2 \pi^2} \tag{31}$$

with c the gluon liberation coefficient which was calculated in [8] to be $c = 2 \ln 2$. Following the same steps as in derivation of Eq. (30) we find contributions to the integral in the denominator of the first line of Eq. (9) of uncorrelated two-particle distribution

$$\begin{aligned}
& \int d^2k_2 d\phi_1 \frac{dN}{d^2k_1 dy_1} \frac{dN}{d^2k_2 dy_2} = \frac{dN}{dy_2} \frac{dN}{k_1 dk_1 dy_1} \\
&= c \frac{C_F^2 S_\perp^2 Q_s^2}{\alpha_s^2 \underline{k}_1^2} \frac{4 K_1}{\pi^4} \int_0^\infty \frac{dz}{z^3} J_0(k_1 z) \left(1 - e^{-z^2 Q_s^2/4}\right)^2 \tag{32}
\end{aligned}$$

and of correlated two-particle distribution

$$\begin{aligned}
& \int d^2k_2 d\phi_1 \frac{dN_{corr}}{d^2k_1 dy_1 d^2k_2 dy_2} \\
&= \frac{N_c C_F S_\perp}{\underline{k}_1^2} \frac{8 K_2}{\pi^3} \int_0^\infty \frac{dz}{z^3} \left(1 - e^{-z^2 Q_s^2/4}\right)^2 J_0(k_1 z) \ln \frac{1}{z\mu}. \tag{33}
\end{aligned}$$

As one can obviously see the integral in Eq. (32) is enhanced by factor of $S_\perp Q_s^2/\alpha_s^2$ as compared to the integral in Eq. (33). This means that the total number of correlated pairs of particles is negligible compared to the number of the uncorrelated pairs given by the square of the total multiplicity. Therefore the correlated contribution from Eq. (33) can be neglected compared to the uncorrelated contribution in Eq. (32).

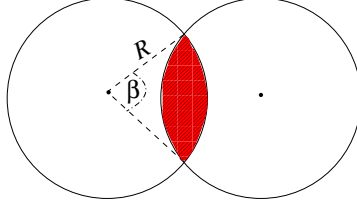


Figure 2: Nuclear collision in the transverse plane.

To estimate the integrals in the second line of Eq. (9) we need to integrate Eq. (30) over momenta k_1

$$\begin{aligned} & \int d^2k_1 d^2k_2 P(k_1, k_2, \underline{B}) \cos(2(\phi_1 - \phi_2)) \\ &= \int_0^\infty dk_1 k_1 \frac{N_c C_F S_\perp}{k_1^2} \frac{4 K_2}{\pi^3} \int_0^\infty \frac{dz}{z^3} \left(1 - e^{-z^2 Q_s^2/4}\right)^2 J_2(k_1 z) \approx \frac{N_c C_F S_\perp Q_s^2 K_2 \ln 2}{2 \pi^3}, \end{aligned} \quad (34)$$

where we assumed that Q_s^2 of Eq. (26) is approximately independent of transverse coordinate z neglecting the logarithm of Eq. (22). To complete the calculation of the integrals in Eq. (9) we note that

$$\int d^2k_1 d^2k_2 P(k_1, k_2, \underline{B}) = \frac{dN}{dy_1} \frac{dN}{dy_2} = \left(c \frac{S_\perp C_F Q_s^2}{\alpha_s 2 \pi^2} \right)^2. \quad (35)$$

Inserting Eqs. (30), (32), (34) and (35) into Eq. (9) and noting that the integration over rapidities is trivial and cancels out between different integrals we obtain

$$v_2(p_T, \underline{B}) = \alpha_s \left(\frac{\pi N_c K_2}{2 \ln 2 C_F S_\perp Q_s^2 K_1^2} \right)^{1/2} \frac{\int_0^\infty \frac{dz}{z^3} J_2(p_T z) \left(1 - e^{-z^2 Q_s^2/4}\right)^2}{\int_0^\infty \frac{dz}{z^3} J_0(p_T z) \left(1 - e^{-z^2 Q_s^2/4}\right)^2}. \quad (36)$$

We have changed the transverse momentum back to p_T to comply with conventional notation. Eq. (36) gives the minijet contribution to the differential elliptic flow for collision of two identical nuclei at given impact parameter \underline{B} . $v_2(p_T)$ measured in experiments is averaged over all impact parameters [22]

$$v_2(p_T) = \frac{\int d^2B v_2(p_T, \underline{B}) (dN/d^2p_T dy)}{\int d^2B (dN/d^2p_T dy)}. \quad (37)$$

In our model each nucleus is cylindrical, so that the dependence on the impact parameter B comes only from the nuclear overlap area $S_\perp(B)$. The overlap area is

$$S_\perp = R^2 (\beta - \sin \beta) = R^2 (2 \arccos(B/2R) - \sin(2 \arccos(B/2R))), \quad (38)$$

where β is the opening angle in the transverse plane as shown in Fig. 2. From Eq. (27) we see that $dN/d^2p_T dy \sim S_\perp(\underline{B})$ and from Eq. (36) one concludes that $v_2(p_T, \underline{B}) \sim 1/\sqrt{S_\perp(\underline{B})}$. Therefore after using Eqs. (27) and (36) in Eq. (37) the impact parameter averaging reduces to

$$\frac{\int_0^{2R} dB B \sqrt{2 \arccos(B/2R) - \sin(2 \arccos(B/2R))}}{R \int_0^{2R} dB B (2 \arccos(B/2R) - \sin(2 \arccos(B/2R)))} \approx \frac{.99}{R} \approx \sqrt{\frac{\pi}{S_\perp^A}}, \quad (39)$$

where $S_{\perp}^A = \pi R^2$ is the cross sectional area of the nucleus. The final result for $v_2(p_T)$ reads

$$v_2(p_T) = \alpha_s \left(\frac{\pi^2 N_c K_2}{2 \ln 2 C_F S_{\perp}^A Q_s^2 K_1^2} \right)^{1/2} \frac{\int_0^{\infty} \frac{dz}{z^3} J_2(p_T z) \left(1 - e^{-z^2 Q_s^2/4}\right)^2}{\int_0^{\infty} \frac{dz}{z^3} J_0(p_T z) \left(1 - e^{-z^2 Q_s^2/4}\right)^2}. \quad (40)$$

Eq. (40) is our main result for differential elliptic flow. Let us first study the qualitative features of the flow from Eq. (40) before using it to fit RHIC data in Sect. 4.

In the small momentum region, $p_T \ll Q_s$, we can neglect the exponents in the numerator and denominator of Eq. (40). Expanding the Bessel functions for small $p_T z$ and cutting off the integrals over z by $1/p_T$ from above and $1/Q_s$ from below we end up with

$$v_2(p_T) \approx \alpha_s \left(\frac{\pi^2 N_c K_2}{2 \ln 2 C_F S_{\perp}^A Q_s^2 K_1^2} \right)^{1/2} \frac{p_T^2}{4 Q_s^2} \ln \frac{Q_s}{p_T}, \quad p_T \ll Q_s. \quad (41)$$

We see that minijet v_2 is an increasing function of transverse momentum, which is in qualitative agreement with the data.

The asymptotic behavior of v_2 at high transverse momenta of the particles, $p_T \gg Q_s$, can be found by expanding the exponents in the numerator and denominator of Eq. (40). Here it is essential to keep logarithms arising from Eqs. (26) and (22). Simple integration yields

$$v_2(p_T) \approx \alpha_s \left(\frac{\pi^2 N_c K_2}{2 \ln 2 C_F S_{\perp}^A Q_s^2 K_1^2} \right)^{1/2} \ln(p_T/\mu), \quad p_T \gg Q_s. \quad (42)$$

Therefore we conclude that while the differential elliptic flow given by Eq. (40) increases for small transverse momenta, at $p_T \sim Q_s$ it turns over and its growth slows down to just a logarithmic increase. As the transverse momentum increases the DGLAP [48] logarithms should become important modifying Eq. (42). The logarithm in Eq. (42) might also be an artifact of our approach and it might disappear if a more detailed analysis is carried out with inclusion of evolution effects in the gluon distribution functions. At the moment we can make an observation that the contribution from minijets to differential elliptic flow is in qualitative agreement with the data [26].

To understand the centrality dependence of the elliptic flow coming from minijets we use the definition [22]

$$v_2(B) = \frac{\int d^2 p_T dy v_2(p_T, \underline{B}) (dN/d^2 p_T dy)}{\int d^2 p_T dy (dN/d^2 p_T dy)} \quad (43)$$

to obtain using Eqs. (27) and (31)

$$v_2(B) = \alpha_s \left(\frac{2 \ln 2 \pi K_2 N_c}{c^2 C_F S_{\perp}(B) Q_s^2} \right)^{1/2}, \quad (44)$$

where $S_{\perp}(B)$ is now the B -dependent nuclear overlap area. Since $S_{\perp}(B) Q_s^2 \sim N_{part}$ we may therefore conclude that minijets flow scales as

$$v_2(B) \sim \frac{1}{\sqrt{N_{part}}}. \quad (45)$$

Elliptic flow from Eq. (45) is smaller for central collisions with large N_{part} and it increases for peripheral collisions with decreasing N_{part} , again in qualitative agreement with the data [21, 22, 23].

4 Our model versus experimental data

There are three interesting kinematical regions in high energy heavy ion collisions corresponding to various values of transverse momenta p_T :

- (i) $p_T \lesssim Q_s$ where multiple rescatterings of partons dominate. In this region transverse momentum dependence of v_2 is given by Eq. (41). Owing to the nonlinear interactions nuclear structure functions in region (i) are functions of only one variable $Q/Q_s(x)$ instead of two Q and x . This is often referred to as geometric scaling [50].
- (ii) $p_T \gg Q_s$ where the DGLAP [48] evolution starts to be important. There the leading behavior of v_2 is given by Eq. (42) in which DGLAP equation may introduce logarithmic corrections, possibly changing the power of $\ln(p_T/\mu)$. The scaling behavior is broken down.
- (iii) At high energies in the course of quantum evolution the saturation scale Q_s becomes much larger than any soft QCD scale Λ . It was argued both analytically [51] and numerically [50, 10, 52] that the geometrical scaling holds in a much wider kinematical region than (i). In fact the additional scaling region is $Q_s \lesssim p_T \lesssim Q_s^2/\Lambda$. Here even though the scattering amplitude is still far from saturation, the nonlinear interactions produce remarkable scaling phenomenon. It was argued in [12] that the saturation scale in RHIC kinematical region is of the order of $1 \div 1.4$ GeV. Since $\Lambda \sim 0.1 \div 0.2$ GeV, we expect the scaling to be important at $p_T \leq 5 \div 10$ GeV, i.e., throughout most of the kinematic region of the differential elliptic flow data [26].

To compare predictions of our model with data collected by the STAR collaboration at RHIC [26] we should evaluate v_2 given by Eq. (40) and Eq. (44) at $p_T < 5$ GeV. This means calculation in the regions (i) and (iii) where geometric scaling works and the only relevant dimensional scale is Q_s . Quantum evolution changes the quasi-classical result of Eq. (26) so that the saturation scale acquires energy dependence. Its analytical expression can be calculated from the nonlinear evolution equation [9]. There is a simple way to introduce Q_s into our model preserving geometric scaling developed by quantum evolution, where Q_s will play a role of a phenomenological parameter which is used to fit the data. Namely, by definition the saturation scale is a scale at which the expression in the Glauber exponent of Eq. (25) equals one

$$\frac{1}{4} \underline{z}^2 Q_s^2(\underline{z}) |_{\underline{z}^2=4/Q_s^2} = \frac{Q_{s0}^2}{Q_s^2} \ln \frac{Q_s}{2\mu} = 1, \quad (46)$$

where we have introduced in the quasi-classical (Glauber) approximation

$$Q_{s0}^2 = \frac{4\pi \alpha_s^2 A}{S_{\perp}^A}, \quad (47)$$

which is an unknown constant for the case of a fully evolved distribution. Q_{s0} can be easily expressed in terms of Q_s using Eq. (46)

$$Q_{s0}^2 = \frac{Q_s^2}{\ln \frac{Q_s}{2\mu}}. \quad (48)$$

Substituting Eq. (48) into Eq. (40) means the following change in the power of the Glauber exponents

$$-\frac{1}{4} z^2 Q_{s0}^2 \ln \frac{1}{z\mu} = -\frac{1}{4} z^2 Q_s^2 \frac{\ln \frac{1}{z\mu}}{\ln(Q_s/2\mu)}. \quad (49)$$

Using Eq. (49) in Eq. (40) we can write for the integrals involved

$$\int_0^\infty \frac{dz}{z^3} J_n(p_T z) \left(1 - e^{-z^2 Q_s^2(z)/4}\right)^2 = p_T^2 \int_0^\infty \frac{d\xi}{\xi^3} J_n(\xi) \left(1 - e^{-(\xi^2 Q_s^2/4p_T^2) \frac{\ln \frac{2p_T}{\xi\Lambda}}{\ln(Q_s/\Lambda)}}\right)^2 \quad (50)$$

where we defined $\xi \equiv p_T z$, $\Lambda = 2\mu$ and $n = 0$ or 2 . Geometric scaling [50] implies that the distribution functions depend only on one parameter p_T/Q_s . To eliminate the scaling violating terms in Eq. (50) we note that the average value $\langle z \rangle \sim 1/\langle p_T \rangle \sim 2/Q_s$ and rewrite the logarithm as

$$\ln \frac{2p_T}{\xi\Lambda} \approx \ln \frac{Q_s}{\xi\Lambda} \quad (51)$$

where Λ would be an independent parameter of our fit restricted by reasonable possible values of the non-perturbative scale. The integral of Eq. (50) becomes

$$p_T^2 \int_0^\infty \frac{d\xi}{\xi^3} J_n(\xi) \left(1 - e^{-(\xi^2 Q_s^2/4p_T^2) \frac{\ln \frac{Q_s}{\xi\Lambda}}{\ln(Q_s/\Lambda)}}\right)^2. \quad (52)$$

This form of the integrals will be used in Eq. (40) to numerically estimate $v_2(p_T)$.

To obtain numerical value of $v_2(p_T)$ we have to estimate the normalization coefficient K_1 . To this aim note that the fraction of the total particle multiplicity per unit of rapidity due to soft saturation physics in heavy ion collisions at center-of-mass energy $\sqrt{s} = 130$ GeV is given by [12]

$$\frac{dN_{sat}}{dy} \approx 1.02 \frac{3 N_{part}}{2}, \quad (53)$$

where $3/2$ is the conversion factor from charged particles to all particles multiplicity. On the other hand, we can calculate the total particle multiplicity by integrating Eq. (27) over all momenta k_1 which gives

$$\frac{dN}{dy} = K_1 \frac{2 \ln 2 S_\perp^A C_F Q_s^2}{\pi^2 \alpha_s} \ln \frac{Q_s}{2\mu}. \quad (54)$$

Equating Eq. (53) and Eq. (54) for the head-on collisions ($B = 0$) we obtain

$$K_1 = \frac{3 \pi^2 \alpha_s 1.02 N_{part}(B=0)}{4 \ln 2 S_\perp^A C_F Q_s^2 \ln(Q_s/\Lambda)}. \quad (55)$$

where $N_{part}(B=0) = 344$ [12]. For gold nuclei with $\alpha_s = 0.3$, $Q_s = 1.0$ GeV and $\Lambda \approx 0.15$ GeV the normalization factor is $K_1 \approx 0.14$.

With the help of Eq. (52) the integration in Eq. (40) has been done numerically for $\Lambda \approx 0.15$ GeV. We put $K_2 = 2$ in Eq. (40) in agreement with collinear factorization approaches [46, 47]. $S_\perp^A = \pi R^2$ with the radius given by Woods–Saxon parameterization $R = 1.1A^{1/3}$ fm. The results are shown in Fig. 3. It can be seen that our model describes the high p_T data

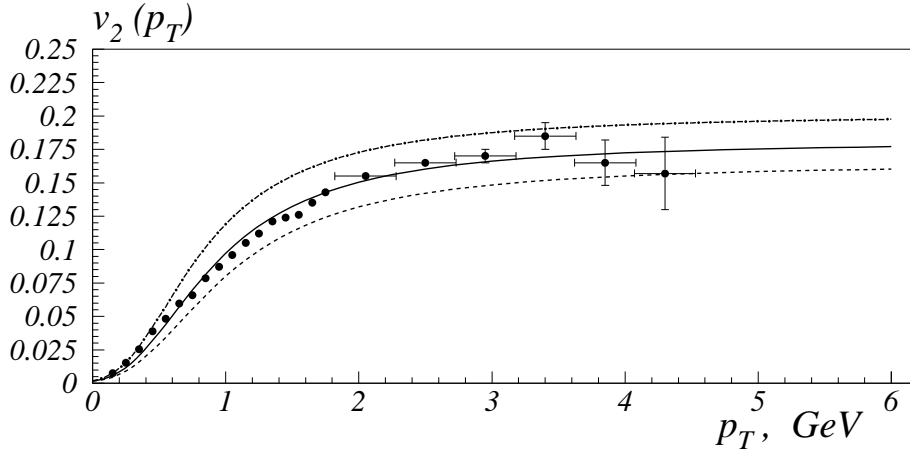


Figure 3: Differential elliptic flow data from STAR [26] versus the predictions of our minijet model. Different lines correspond to our predictions with different values of the saturation scale: $Q_s = 1.0$ GeV (solid line), $Q_s = 1.1$ GeV (dashed line) and $Q_s = 0.9$ GeV (dash-dotted line). We used the following parameters $\Lambda=0.15$ GeV, $\alpha_s=0.3$, $A=197$ (Gold).

remarkably well. We are led to the conclusion that the high momentum tail of the v_2 is saturated by the two-particle correlated minijet production. We can also explain the turnover of v_2 at $p_T \sim 1 \div 2 \sim Q_s$ GeV as being due to saturation effects in the wave functions of the colliding nuclei at low p_T . Another important observation is that two-particle correlations in the initial state give significant contribution at low p_T as one can see in Fig. 3. Note that the p_T^2 increase of v_2 at small momenta may be an artifact of our model which neglects the change of the anomalous dimension γ of the gluon structure function. It is well known that correct anomalous dimension at the boundary of the saturation region is $\gamma \approx 1/2$ [10]. It smoothly changes from 0 in the unitarity limit to 1 in the Bjorken limit [10]. More accurate analysis is needed to understand the low p_T behavior of v_2 due to two-particle correlations in minijet production.

Applicability of our model is restricted to the mid-rapidity kinematical region. However, since the total particle multiplicity is dominated by the particle production at mid-rapidity the averaging over all impact parameters in Eq. (37) gives a reasonable approximation. The situation is different if we want to apply our model to describe the centrality dependence of v_2 . While we expect it to be in agreement with the data for the most central events, it is not legitimate to use it for peripheral collisions.

Eqs. (44) and (45) imply

$$v_2(B) = \frac{v_2(B=0) \sqrt{N_{\text{part}}(B=0)}}{\sqrt{N_{\text{part}}}} = \alpha_s \left(\frac{\pi N_c K_2 N_{\text{part}}(B=0)}{2 \ln 2 C_F S_{\perp}^A Q_s^2 N_{\text{part}}} \right)^{1/2}, \quad (56)$$

where we used $c = 2 \ln 2$ [8]. In Fig. 4 we show the result of numerical calculations compared to STAR data [22, 26]. The data is represented by black dots while our fit is given by empty crosses. We have used Eq. (56) with the coefficient $K_2 = 2$. To find the average N_{part} in a

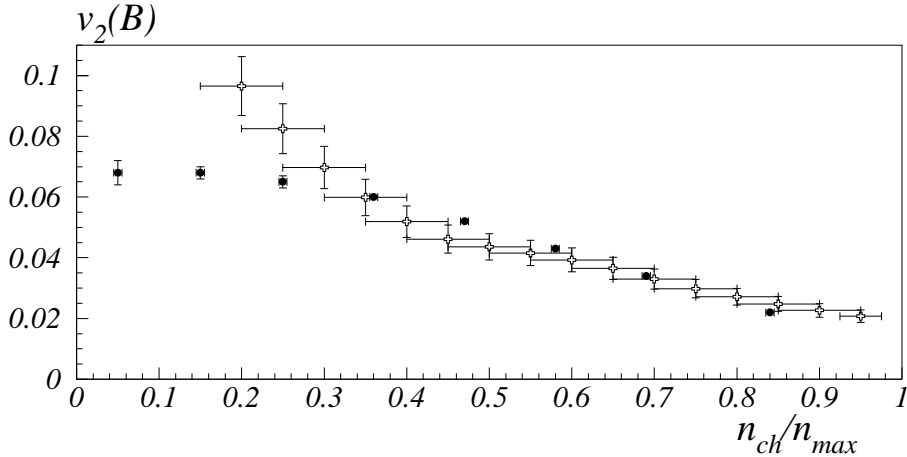


Figure 4: Centrality dependence of elliptic flow given by the STAR data (black dots) and our fit (empty crosses). We used $\Lambda=0.15$ GeV, $\alpha_s=0.3$, $A=197$, $Q_s=1$ GeV and $N_{\text{part}}(B=0) = 344$ [12].

given centrality bin we have used the model of Kharzeev and Nardi [12]. Horizontal error bars in our fit correspond to the widths of centrality bins. Vertical error bars account for our use of cylindrical nuclear shape instead of spherical and for the uncertainty in N_{part} coming from the model of [12]. As expected our model provides a reasonable description of the data for central events while the fit does not work that well for peripheral collisions. The saturation scale decreases toward the large impact parameters where at some point it becomes of the order of Λ_{QCD} and the small coupling approach breaks down. Thus, as was mentioned above, our approach is not applicable to very peripheral collisions and can not be expected to work for them. We conclude that our model gives a reasonable description of v_2 centrality dependence for the values of centrality $n_{ch}/n_{max} \geq 0.4$.

The maximum of the centrality distribution of elliptic flow is probably determined by the onset of non-perturbative effects. The flow from Eq. (44) increases with increasing B , until at some point the saturation scale $Q_s(B)$ becomes of the order of Λ_{QCD} and non-perturbative effects take over keeping $v_2(B)$ approximately constant for peripheral collisions. (Strictly speaking Eq. (44) was derived for cylindrical nuclei with saturation scales independent of the impact parameter. However in real life Q_s is of course a function of B [38, 12, 13].) Let us denote the impact parameter at which the non-perturbative effects take over by B_0 , so that $Q_s(B_0) \approx \Lambda_{QCD}$. Since Q_s is an increasing function of the center of mass energy s [9, 10], the impact parameter B_0 must also be an increasing function of s . That is as energy increases more and more collisions become perturbative with the non-perturbative physics being responsible only for increasingly more peripheral collisions. The maximum of the flow centrality distribution could be estimated from Eq. (44) to be $v_2(B_0) \sim 1/\sqrt{S_{\perp}(B_0)\Lambda_{QCD}^2}$. With the increase of energy B_0 increases, $S_{\perp}(B_0)$ decreases and, therefore, $v_2(B_0)$ increases, which qualitatively agrees with RHIC and SPS data [26, 19, 20, 21, 22, 23].

5 Conclusions

In this paper we have calculated the contribution of pairwise azimuthal correlations in minijet production to elliptic flow variable. The resulting differential elliptic flow $v_2(p_T)$ given by Eq. (40) is in good qualitative (see Eqs. (41) and (42)) and quantitative (see Fig. 3) agreement with the emerging RHIC data [21, 22, 23, 26]. The centrality dependence of the minijet contribution to elliptic flow $v_2(B)$ (see Eqs. (44) and (45)) successfully describes the data for sufficiently central collisions as shown in Fig. 4. The maximum $v_2(B)$ appears to increase with energy also in agreement with the data [26].

There are several important questions which still have to be addressed in the future as more flow data is produced at RHIC. One question concerns the value of the directed flow v_1 . It may seem from the above discussion that using two-particle correlations one might write, similar to Eq. (6),

$$v_1(p_T) = \frac{\langle \cos(\phi_1(p_T) - \phi_2) \rangle}{\sqrt{\langle \cos(\phi_1 - \phi_2) \rangle}} \quad (57)$$

and using the correlations of Eq. (28) get a non-zero directed flow. However, let us remind the reader that in the analysis of directed flow the signs of the weights used in determination of the reaction plane are reversed in backward hemisphere with respect to the forward one [18, 31]. That is, in the numerator of Eq. (57), the contributions from $y_2 > 0$ and $y_2 < 0$ come in with different signs (we denote the central rapidity of the event by $y = 0$). Therefore, since in our boost-invariant model the two contributions are identical, the final result for v_1 at mid-rapidity is zero in agreement with the SPS data [19]. If we impose some constraint on the rapidity interval of the analyzed particles making it asymmetric with respect to $y = 0$, e.g. analyzing only particles with $y > 0$, the differential directed flow from minijets would also become non-zero as observed experimentally [19].

In our analysis we have neglected contributions from correlated production of three and more particles in a single subcollision. The corresponding diagrams may also contribute to the two-particle correlation function in Eq. (8). Of course they are suppressed by extra powers of the strong coupling constant α_s compared to Eq. (28), though these extra powers are compensated by the large logarithms arising due to phase space integration [48, 42]. In heavy ion collisions at RHIC the saturation scale is of the order of $Q_s \sim 1$ GeV [12, 13, 8] and the corresponding value of the coupling constant is $\alpha_s(Q_s) \approx 0.3$, which is not too small and will also be enhanced by logarithms of energy and transverse momentum. Thus to have a precise description of the minijet contribution to elliptic flow one has to resum all these multiple emission diagrams, which is equivalent to including the effects of quantum evolution in the double inclusive gluon distribution of Eq. (28). Since at the moment there is even no rigorously derived expression for double gluon production in AA in the quasi-classical approximation, including evolution effects in it seems like an important but not immediate goal.

To improve the quality of the minijet predictions one has to also relax the $y_1 \gg y_2$ (or $y_1 \ll y_2$) condition which we imposed to simplify the calculation. This condition led to absence of rapidity correlations in the two-particle distribution given by our Eq. (24). Also the azimuthal correlations given by Eq. (24) are only “back-to-back”, i.e., the produced particles are correlated mostly in the opposite directions in the transverse plane. This behavior seems to contradict recent results reported by PHENIX [23, 53] where the two-particle correlation function $C(\Delta\phi =$

$\phi_1 - \phi_2$) has maxima at both $\Delta\phi = \pi$ (back-to-back) and $\Delta\phi = 0$. Relaxing the $y_1 \gg y_2$ (or $y_1 \ll y_2$) condition would greatly complicate the particle production calculations [43] though would give predictions for elliptic flow in a much more realistic kinematics. The appropriate calculations were performed for production of a pair of particles with $y_1 \sim y_2$ by Leonidov and Ostrovsky in [44]. The results of [44] indicate that the two produced particles are indeed somewhat correlated in rapidity. The analysis of azimuthal distributions performed in [44] also demonstrates enhancement of both $\Delta\phi = \pi$ and $\Delta\phi = 0$ correlations in the obtained double particle spectrum, in qualitative agreement with PHENIX data [23, 53]. These correlations should also contribute to smallness of directed flow v_1 . A detailed analysis of elliptic flow employing the full calculation of [44] will be done elsewhere [54]. In a complete analysis one has to put in realistic geometrical shapes for the nuclei as well. Of course the effects of different cuts used to analyze the data and various choices of weights have to be incorporated in the precise analysis too. While these modifications are likely to introduce some numerical changes in the fits to the elliptic flow data presented above, we believe that the qualitative conclusions of importance of the minijet production to flow variables would remain unchanged.

We therefore conclude that minijets give a large contribution to the elliptic flow extracted using current flow analysis methods, probably accounting for most of the flow at large p_T (see Fig. 3). Differential elliptic flow appears to be sensitive to saturation physics of the early stages of the collisions. To study QGP it would be very useful to invent a method of flow analysis that would be insensitive to minijet contribution and would only measure the collective effects due to elliptic flow [32, 33]. We have to note, however, that if one tries to calculate the double inclusive minijet production cross section in the saturation approach [2, 6, 8] many of the diagrams that would contribute would reduce to independent production of two gluons which would then exchange a gluon with each other. This $2 \rightarrow 2$ process would constitute the first step in the onset of thermalization [16]. Therefore it appears that correlated production of pairs of minijets may be intrinsically related to thermalization. On one hand this implies that the minijet flow of Eq. (40) is partially due to collective effects after all. On the other hand it may be impossible to create an observable which would distinguish these early stage thermalization effects from the flow of the fully thermalized quark-gluon plasma.

Acknowledgements

The authors would like to thank Adrian Dumitru, Miklos Gyulassy, Dima Kharzeev, Roy Lacey, Larry McLerran, Jean-Yves Ollitrault, and Jan Rak for stimulating and informative discussions. Our thanks go to Derek Teaney and Raju Venugopalan for pointing out to us a numerical error in the earlier version of the paper.

The work of Yu. K. was supported in part by the U.S. Department of Energy under Grant No. DE-FG03-97ER41014 and by the BSF grant # 9800276 with Israeli Science Foundation, founded by the Israeli Academy of Science and Humanities. The work of K. T. was sponsored in part by the U.S. Department of Energy under Grant No. DE-FG03-00ER41132.

References

- [1] L. V. Gribov, E. M. Levin, and M. G. Ryskin, Phys. Rep. **100**, 1 (1983); A.H. Mueller, J.-W. Qiu, Nucl. Phys. **B268**, 427 (1986).
- [2] L. McLerran and R. Venugopalan, Phys. Rev. D **49**, 2233 (1994); **49**, 3352 (1994); **50**, 2225 (1994).
- [3] E.V. Shuryak, Phys. Lett. **B78**, 150 (1978); L.D. McLerran, B. Svetitsky, Phys. Rev. D **24**, 450 (1981).
- [4] Yu.V. Kovchegov, Phys. Rev. D **54**, 5463 (1996); **55**, 5445 (1997).
- [5] J. Jalilian-Marian, A. Kovner, L. McLerran, and H. Weigert, Phys. Rev. D **55**, 5414 (1997).
- [6] A. Kovner, L. McLerran, and H. Weigert, Phys. Rev. D **52**, 6231 (1995); **52**, 3809 (1995); M. Gyulassy, L. McLerran, Phys. Rev. C **56**, 2219 (1997); Yu.V. Kovchegov, D. H. Rischke, Phys. Rev. C **56**, 1084 (1997); X. Guo, Phys. Rev. D **59**, 094017 (1999).
- [7] A. Krasnitz, R. Venugopalan, Report No. hep-ph/0007108; Phys. Rev. Lett. **84**, 4309 (2000); Nucl. Phys. **B557**, 237 (1999); A. Krasnitz, Y. Nara, R. Venugopalan, Phys. Rev. Lett. **87**, 192302 (2001).
- [8] Yu. V. Kovchegov, Nucl. Phys. **A692**, 557 (2001); Nucl. Phys. **A698**, 619c (2002).
- [9] I. I. Balitsky, Report No. hep-ph/9706411; Nucl. Phys. **B463**, 99 (1996); Phys. Rev. D **60**, 014020 (1999); Yu. V. Kovchegov, Phys. Rev. D **60**, 034008 (1999); D **61**, 074018 (2000).
- [10] E. Levin and K. Tuchin, Nucl. Phys. **B573**, 833 (2000); Nucl. Phys. **A691**, 779 (2001); Nucl. Phys. **A693**, 787 (2001); M. A. Braun, Eur. Phys. J. C **16**, 337 (2000); hep-ph/0010041; hep-ph/0101070; K. Golec-Biernat, L. Motyka, A.M. Stasto, hep-ph/0110325.
- [11] J. Jalilian-Marian, A. Kovner, A. Leonidov, and H. Weigert, Phys. Rev. **D59**, 034007 (1999); E. Ferreira, E. Iancu, A. Leonidov, L. McLerran, hep-ph/0109115 and references therein.
- [12] D. Kharzeev, M. Nardi, Phys. Lett. **B507**, 121 (2001).
- [13] D. Kharzeev, E. Levin, Phys. Lett. **B523**, 79 (2001); D. Kharzeev, E. Levin, M. Nardi, hep-ph/0111315.
- [14] B. Müller, Rep. Prog. Phys. **58**, 611 (1995).
- [15] F. Karsch, Nucl. Phys. B (Proc. Suppl.) **34**, 63 (1994); Phys. Rev. D **49**, 3791 (1994); E. Laermann, Nucl. Phys. **A610**, 1c (1996).
- [16] R. Baier, A.H. Mueller, D. Schiff, D.T. Son, Phys. Lett. **B502**, 51 (2001); A.H. Mueller, Phys. Lett. **B475**, 220 (2000); Nucl. Phys. **B572**, 227 (2000).
- [17] Yu. V. Kovchegov, E. Levin, L. D. McLerran, Phys. Rev. C **63**, 024903 (2001).

- [18] M. Gyulassy, K. A. Frankel, and H. Stöcker, Phys. Lett, **110B**, 185 (1982); P. Danielewicz and G. Odyniec, Phys. Lett. **B157**, 146 (1985); J.-Y. Ollitrault, Phys. Rev. D **46**, 229 (1992); for a review, see J.-Y. Ollitrault, Nucl. Phys. **A638**, 195c (1998).
- [19] H. Appelshäuser *et al.*, (NA49 Collaboration), Phys. Rev. Lett. **80**, 4136 (1998).
- [20] M. M. Aggarwal *et al.*, (WA98 Collaboration), Nucl. Phys. **A663**, 729 (2000).
- [21] Inkyu C. Park for the PHOBOS Collaboration, Nucl. Phys. **A698**, 564 (2002).
- [22] STAR Collaboration, K.H. Ackermann *et al.*, Phys. Rev. Lett. **86**, 402 (2001); STAR Collaboration, C. Adler *et al.*, Phys. Rev. Lett. **87**, 182301 (2001).
- [23] Roy A. Lacey for the PHENIX Collaboration, Nucl. Phys. **A698**, 559 (2002).
- [24] P.F. Kolb, U. W. Heinz, P. Huovinen, K.J. Eskola, K. Tuominen, Nucl. Phys. **A696**, 197 (2001); P. Huovinen, P.F. Kolb, U. W. Heinz, P.V. Ruuskanen, S.A. Voloshin, Phys. Lett. **B503**, 58 (2001); P.F. Kolb, P. Huovinen, U. W. Heinz, H. Heiselberg, Phys. Lett. **B500**, 232 (2001).
- [25] D. Teaney and E.V. Shuryak, Phys. Rev. Lett. **83** (1999) 4951; D. Teaney, J. Lauret, E.V. Shuryak, nucl-th/0110037; Phys. Rev. Lett. **86**, 4783 (2001).
- [26] R.J.M. Snellings for the STAR Collaboration, Nucl. Phys. **A698**, 193 (2002).
- [27] M. Gyulassy, I. Vitev, X.-N. Wang, Phys. Rev. Lett. **86**, 2537 (2001); X.-N. Wang, Phys. Rev. C **63**, 054902 (2001); M. Gyulassy, I. Vitev, X.-N. Wang, P. Huovinen, Phys. Lett. **B526**, 301 (2002); D. Molnar, M. Gyulassy, Nucl. Phys. **A697**, 495 (2002).
- [28] M. Gyulassy, P. Levai, I. Vitev, Phys. Rev. Lett. **85**, 5535 (2000) and references therein; R. Baier, Y. L. Dokshitzer, A. H. Mueller and D. Schiff, JHEP **0109**, 033 (2001) and references therein.
- [29] D. Teaney, R. Venugopalan, hep-ph/0203208.
- [30] S. Voloshin, Y. Zhang, Z. Phys. **C70**, 665 (1996).
- [31] A.M. Poskanzer, S.A. Voloshin, Phys. Rev. C **58**, 1671 (1998) and references therein.
- [32] N. Borghini, P. M. Dinh, J.-Y. Ollitrault, Phys. Rev. C **63**, 054906 (2001); C **64**, 054901 (2001); hep-ph/0111402.
- [33] N. Borghini, P. M. Dinh, J.-Y. Ollitrault, Phys. Rev. C **62**, 034902 (2000); P. M. Dinh, N. Borghini, J.-Y. Ollitrault, Phys. Lett. **B477**, 51 (2000).
- [34] S. Wang *et al.*, Phys. Rev. C **44**, 1091 (1991).
- [35] N. Borghini, P. M. Dinh, J.-Y. Ollitrault, A.M. Poskanzer, S.A. Voloshin, nucl-th/0202013.
- [36] A.H. Tang, hep-ex/0108029.

- [37] A.H. Mueller, Nucl. Phys. **B335**, 115 (1990).
- [38] Yu. V. Kovchegov, A.H. Mueller, Nucl. Phys. **B529**, 451 (1998).
- [39] Yu. V. Kovchegov, K. Tuchin, hep-ph/0111362.
- [40] J. P. Blaizot, A. H. Mueller, Nucl. Phys. **B 289**, 847 (1987); K. J. Eskola, K. Kajantie, and J. Lindfors, Nucl. Phys. **B 323**, 37 (1989).
- [41] K. J. Eskola, V.J. Kolhinen, and P.V. Ruuskanen, Nucl. Phys. **B 535**, 351 (1998); K.J. Eskola, V.J. Kolhinen, C.A. Salgado, Eur. Phys. J. **C9**, 61 (1999); N. Hammon, H. Stocker, W. Greiner, Phys. Rev. C **61**, 014901 (2000).
- [42] E.A. Kuraev, L.N. Lipatov and V.S. Fadin, *Sov. Phys. JETP* **45**, 199 (1977); Ya.Ya. Balitsky and L.N. Lipatov, *Sov. J. Nucl. Phys.* **28**, 22 (1978).
- [43] V.S. Fadin and L.N. Lipatov, Phys. Lett. B **429**, 127 (1998); M. Ciafaloni and G. Camici, Phys. Lett. B **430**, 349 (1998).
- [44] A. Leonidov and D. Ostrovsky, Phys. Rev. D **62**, 094009 (2000); hep-ph/9811417; Eur. Phys. J. **C11**, 495 (1999); Eur. Phys. J. **C16**, 683 (2000).
- [45] E.M. Levin, M.G. Ryskin, Yad. Fiz. **21**, 1072 (1975).
- [46] K.J. Eskola, K. Kajantie, P.V. Ruuskanen, K. Tuominen, hep-ph/0204034; K.J. Eskola, K. Kajantie, K. Tuominen, Nucl. Phys. **A700**, 509 (2002).
- [47] M. Gyulassy, X.-N. Wang, Phys. Rev. D **44**, 3501 (1991); Phys. Rev. D **45**, 844 (1992); Comput. Phys. Commun. **83**, 307 (1994).
- [48] V.N. Gribov and L.N. Lipatov, Sov. J. Nucl. Phys. **15**, 438 (1972); G. Altarelli and G. Parisi, Nucl. Phys. **B 126**, 298 (1977); Yu.L. Dokshitzer, Sov. Phys. JETP **46**, 641 (1977).
- [49] A.H. Mueller, Nucl. Phys. **B572**, 227 (2000).
- [50] A.M. Stasto, K. Golec-Biernat and J. Kwiecinski, Phys. Rev. Lett. **86**, 596 (2001).
- [51] E. Iancu, K. Itakura, L. McLerran, hep-ph/0203137.
- [52] E. Levin and M. Lublinsky, Nucl. Phys. **A696**, 833 (2001); M. Lublinsky, Eur. Phys. J. **C21**, 513 (2001).
- [53] PHENIX Collaboration, K. Adcox et al, nucl-ex/0204005; J. Rak, *High- p_T charged particles azimuthal correlation in PHENIX*, Proceedings of the International Workshop XXX on Gross Properties of Nuclei and Nuclear Excitations Hirscheegg, Austria, 2002; R. A. Lacey, *Elliptic Flow Measurements with the PHENIX Detector*, Proceedings of the 15th International Conference on Ultrarelativistic Nucleus-Nucleus Collisions (QM2001), Stony Brook, New York, 2001, Nucl. Phys. **A698**, 559 (2002).
- [54] Yu. V. Kovchegov, K. L. Tuchin, in preparation.